Journal of Geophysical Research: Atmospheres

RESEARCH ARTICLE
10.1029/2018JD028901

Radiosondes Show That After Decades of Cooling, the Lower Stratosphere Is Now Warming

Rolf Philipona[1], Carl Mears[2], Masatomo Fujiwara[3], Pierre Jeannet[1], Peter Thorne[4], Greg Bodeker[5], Leopold Haimberger[6], Maxime Hervo[7], Christoph Popp[7], Gonzague Romanens[7], Wolfgang Steinbrecht[8], Rene Stübi[7], and Roeland Van Malderen[9]

[1]Federal Office of Meteorology and Climatology MeteoSwiss (retired), Payerne, Switzerland, [2]Remote Sensing Systems, Santa Rosa, CA, USA, [3]Faculty of Environmental Earth Science, Hokkaido University, Sapporo, Japan, [4]Department of Geography, Maynooth University, Maynooth, Ireland, [5]Bodeker Scientific, Alexandra, New Zealand, [6]Department of Meteorology and Geophysics, University of Vienna, Vienna, Austria, [7]Federal Office of Meteorology and Climatology MeteoSwiss, Payerne, Switzerland, [8]German Weather Service, Meteorological Observatory Hohenpeissenberg, Germany, [9]Royal Meteorological Institute of Belgium, Uccle, Belgium

Abstract Since the mid-twentieth century, radiosonde and satellite measurements show that the troposphere has warmed and the stratosphere has cooled. These changes are primarily due to increasing concentrations of well-mixed greenhouse gases and the depletion of stratospheric ozone. In response to continued greenhouse gas increases and stratospheric ozone depletion, climate models project continued tropospheric warming and stratospheric cooling over the coming decades. Global average satellite observations of lower stratospheric temperatures exhibit no significant trends since the turn of the century. In contrast, an analysis of vertically resolved radiosonde measurements from 60 stations shows an increase of lower stratospheric temperature since the turn of the century at altitudes between 15 and 30 km and over most continents. Trend estimates are somewhat sensitive to homogeneity assessment choices, but all investigated radiosonde data sets suggest a change from late twentieth century cooling to early 21st century warming in the lower stratosphere, which is consistent with a reversal from ozone depletion to recovery from the effects of ozone-depleting substances. In comparison, satellite observations at the radiosonde locations show only minor early 21st century warming, possibly due to the compensating effects of continued cooling above the radiosonde altitude range.

Key Points:
- Radiosonde profiles show that after decades of cooling, the lower stratosphere is now warming
- Over all continents radiosonde measured TLS trends since 2000 are larger than satellite-observed trends

Correspondence to:
R. Philipona,
rolf.philipona@gmail.com

Citation:
Philipona, R., Mears, C., Fujiwara, M., Jeannet, P., Thorne, P., Bodeker, G., et al. (2018). Radiosondes show that after decades of cooling, the lower stratosphere is now warming. *Journal of Geophysical Research: Atmospheres*, *123*, 12,509–12,522. https://doi.org/10.1029/2018JD028901

Received 30 APR 2018
Accepted 17 OCT 2018
Accepted article online 23 OCT 2018
Published online 19 NOV 2018

Author Contributions:
Conceptualization: Rolf Philipona, Masatomo Fujiwara, Peter Thorne
Data curation: Rolf Philipona, Carl Mears, Pierre Jeannet, Leopold Haimberger, Maxime Hervo, Christoph Popp, Gonzague Romanens, Wolfgang Steinbrecht, Rene Stübi, Roeland Van Malderen
Formal analysis: Rolf Philipona, Carl Mears, Pierre Jeannet
Investigation: Rolf Philipona
Methodology: Rolf Philipona, Greg Bodeker
Supervision: Rolf Philipona, Masatomo Fujiwara
Validation: Rolf Philipona, Carl Mears
Visualization: Rolf Philipona
Writing - original draft: Rolf Philipona
Writing – review & editing: Rolf Philipona, Carl Mears, Masatomo Fujiwara, Pierre Jeannet, Peter Thorne, Greg Bodeker, Leopold Haimberger, Wolfgang Steinbrecht, Rene Stübi, Roeland Van Malderen

1. Introduction

Based on multiple independent analyses of measurements from radiosondes and satellite sensors, the global troposphere (below ~12 km) has warmed and the global stratosphere (above ~12 km) has cooled since the mid-1970s (Intergovernmental Panel on Climate Change [IPCC], 2013; Ramaswamy et al., 2001, 2006; Randel et al., 2009; Seidel et al., 2011; Thompson et al., 2012; World Meteorological Organization [WMO], 2014). These temperature changes have been attributed to a combination of the radiative effects of rising greenhouse gas (GHG) concentrations, pre-2000 increases in ozone-depleting substances (ODSs) and post-2000 ODS declines, changing water vapor and aerosol concentrations, and thermal responses to resulting changes in atmospheric dynamics (Butchart, 2014; Langematz et al., 2003; Santer et al., 2003, 2013; Shine et al., 2003, 2008; Solomon et al., 2010).

Globally representative radiosonde records extend back to 1958. Balloon-borne radiosondes measure temperature as the balloon ascends and data are typically provided at standard pressure levels. Satellites have monitored tropospheric and lower stratospheric temperature since late 1978 using the Microwave Sounding Unit (MSU) and the Stratospheric Sounding Unit (SSU) instruments. The follow-on to MSU in 1998 was the Advanced Microwave Sounding Unit (AMSU; Randel et al., 2009; Thompson et al., 2012). MSU/AMSU and SSU retrievals represent vertically integrated temperatures over deep atmospheric layers centered at altitudes from the midtroposphere to the lower (MSU/AMSU) and middle to upper (SSU) stratosphere (IPCC, 2013; Seidel et al., 2011). Most recent analyses of these satellite measurements have shown that stratospheric temperatures steadily decreased to the end of the twentieth century, but since then little change has occurred in the lower stratosphere (McLandress et al., 2015; Randel et al., 2016; Seidel et al., 2016).

The late twentieth century cooling is simulated by models participating in phase 5 of the Coupled Model Intercomparison Project (CMIP5; Thompson et al., 2012; Zhao et al., 2016). Global climate models project further stratospheric cooling (Shepherd & Jonsson, 2008; Thompson & Solomon, 2009) or statistically insignificant trends over the coming decades (Ferraro et al., 2015; Stolarski et al., 2010). By isolating the roles of different forcing agents, models attribute the observed cooling of the middle and upper stratosphere primarily to rising concentrations of GHGs. In the lower stratosphere, changes in ODSs have a clearly detectable influence on ozone. Other influences (such as volcanic effects) are also detectable (Aquila et al., 2016; Bandoro et al., 2018; Gillett et al., 2011; Polvani et al., 2017).

This paper first presents an analysis of upper-air radiosonde temperature profiles from 1976 to 2015, which provides evidence that after decades of cooling, the lower stratosphere is now warming. Lower stratospheric temperature trends from 2001 to 2015 are positive over large parts of the continents and are statistically significant at the 5% level, particularly in midlatitude regions. Over Antarctic stations the lower stratosphere is still cooling. We used temperature records from 52 radiosonde stations that broadly cover the continents of the Northern Hemisphere, and from eight stations in Australia, New Zealand, and Antarctica. Zonal and meridional means are calculated by averaging results from individual stations. The stations were selected according to their long-term data availability. All stations are part of the Global Climate Observing System (GCOS) GCOS Upper Air Network (GUAN, 2014) and the GCOS Reference Upper-Air Network (GRUAN; Bodeker et al., 2016).

In a second step, we compare gridded satellite data with collocated radiosonde data, that are weighted with satellite weighting functions. We use MSU Channel 4 data from 1979 to 1998 and AMSU Channel 9 data from 1998 to 2015. These channels provide information on the temperature of the lower stratosphere (TLS). Advanced Microwave Sounding Unit-A (AMSUA) Channel 10 data from 1998 to 2015 are also used. While some regions also show slight warming trends in satellite TLS data during the period from 2000 to 2015, the satellite observations generally exhibit considerably less warming than the weighted radiosonde measurements.

2. Global Upper-Air Radiosonde Records Used

The radiosonde records used are from IGRA (Integrated Global Radiosonde Archive; Durre et al., 2006), the RAOBCORE (RAdiosonde OBservation COrrection using REanalyses) project (Haimberger, 2007), and the IUK (Iterative Universal Kriging; Sherwood & Nishant, 2015) data set. IGRA provides nonhomogenized monthly means for many radiosonde stations. The RAOBCORE data set comprises homogenized radiosonde data for individual radiosonde stations and is produced at the University of Vienna. It uses European Centre for Medium-Range Weather Forecasts (ECMWF) ERA-interim reanalyses (Dee et al., 2011) to identify and adjust for inhomogeneities in the station records. Two versions of the RICH (Radiosonde Innovation Composite Homogenization; Haimberger et al., 2012) data sets, RICH-obs and RICH-tau, were also used. These data are also from the University of Vienna and are gridded 10° × 10° monthly mean values. Relative to RAOBCORE, the two RICH products use homogeneous neighbor segments. RICH-obs uses the difference series between neighbors, whereas RICH-tau uses the observation minus reanalysis background series differences between stations. IUK is a homogenized data set from the University of New South Wales, Sydney. The homogenization approach employed in IUK is methodologically distinct from that of the University of Vienna products in both breakpoint identification and adjustment approaches.

Together, the family of radiosonde products considered incorporates a broad range of approaches to identifying and adjusting for identified biases and drifts in the underlying records. Combined daytime and nighttime monthly means on 10 standard reporting levels are used. The three station data sets (IGRA, RAOBCORE, and IUK) are compared against each other and against RICH data extracted from the associated 10° × 10° grid point closest to each station.

The 60 radiosonde stations used are shown in Figure 1, and their relevant geographical information is given in Table 1. The Northern Hemisphere is divided into eight regions separated into 30° latitudinal bands and with longitudinal separation between North America, Europe/Africa, and Asia. In the Southern Hemisphere, only few stations have sufficiently long records. Darwin as a tropical station shows comparable trends to the three stations further south. Therefore, the four stations from Australia and New Zealand have been analyzed as one 0–60° southern latitude band. Antarctica is analyzed with four stations.

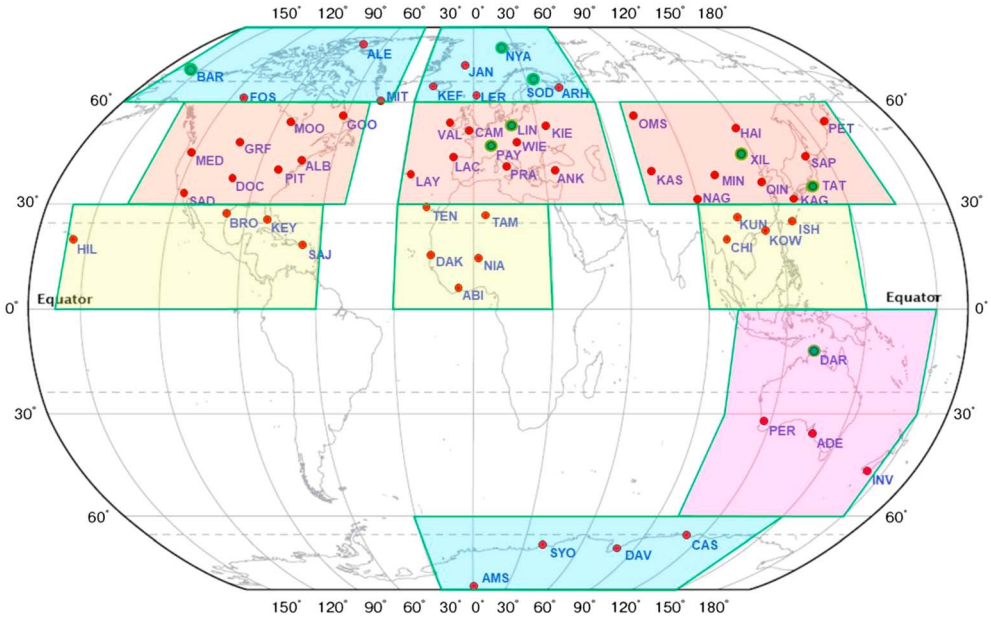

Figure 1. GUAN and GRUAN upper-air stations in 10 regions. The 52 GUAN stations are indicated by red dots and the 8 GRUAN stations by green dots. The stations were selected according to their long-term data availability in the IGRA, RAOBCORE and IUK data sets. Homogenized RICH data are used from the grid box closest to each station location. The Northern Hemisphere is generally well covered with 52 stations, except for northern Asia, where few stations with long records are available. Southern Hemisphere data are much more sparse.

Table 1
GUAN and GRUAN Stations Used for the Analysis

Region	#	Station	Town	Country	WMO- Nb	Lat	Lon	Alt
30–60 EUR	1	LAJ	LAJES (AZORES)	P	8508	38.77	−27.09	73
	2	LAC	LA CORUNA	E	8001	43.37	−8.42	58
	3	VAL	VALENTIA	IRL	3953	51.94	−10.24	24
	4	CAM	CAMBORNE	GB	3808	50.22	−5.33	87
	5	PAY	PAYERNE	CH	6610	46.81	6.94	490
	6	WIE	WIEN	A	11035	48.25	16.36	200
	7	LIN	LINDENBERG	D	10393	52.22	14.12	112
	8	PRA	PRATICA DI MARE	I	16245	41.67	12.45	32
	9	ANK	ANKARA	TR	17130	39.95	32.88	891
	10	KIE	KIEV	UA	33345	50.40	30.57	166
60–90 EUR	1	KEF	KEFLAVIK	IS	4018	63.98	−22.60	52
	2	JAN	JAN MAYEN	N	1001	70.94	−8.67	9
	3	LER	LERWICK	GB	3005	60.14	−1.18	82
	4	NYA	NY-ALESUND	N	1004	78.92	11.92	16
	5	SOD	SODANKYLA	FIN	2836	67.37	26.63	179
	6	ARH	ARHANGEL'SK	RUS	22543	64.62	40.51	4
0–30 AFR	1	TEN	TENERIFE	E	60018	28.32	−16.38	105
	2	DAK	DAKAR	SN	61641	14.73	−17.50	25
	3	ABI	ABIDJAN	CI	65578	5.25	−3.93	7
	4	NIA	NIAMEY	RN	61052	13.48	2.17	223
	5	TAM	TAMANRASSET	DZ	60680	22.80	5.43	1377
30–60 NAM	1	MED	MEDFORD	USA	72597	42.38	−122.88	398
	2	SAD	SAN DIEGO	USA	72293	32.83	−117.12	134
	3	GRF	GREAT FALLS	USA	72776	47.46	−111.38	1132
	4	DOC	DODGE CITY	USA	72451	37.76	−99.97	786
	5	PIT	PITTSBURGH	USA	72520	40.53	−80.22	361
	6	ALB	ALBANY	USA	72518	42.69	−73.83	93
	7	MOO	MOOSONEE	CDN	71836	51.27	−80.65	10
	8	GOO	GOOSE	CDN	71816	53.30	−60.37	36

Table 1 *(continued)*

Region	#	Station	Town	Country	WMO- Nb	Lat	Lon	Alt
60–90 NAM	1	BAR	BARROW	USA	70026	71.29	−156.78	12
	2	FOS	FORT SMITH	CDN	71934	60.03	−111.93	204
	3	MIT	MITTARFIK	GL	4270	61.17	−45.42	34
	4	ALE	ALERT	CDN	71082	82.50	−62.33	65
0–30 NAM	1	BRO	BROWNSVILLE	USA	72250	25.92	−97.42	7
	2	KEY	KEY WEST	USA	72201	24.55	−81.76	2
	3	HIL	HILO	USA	91285	19.72	−155.06	11
	4	SAJ	SAN JUAN	PRI	78526	18.43	−65.99	4
30–60 ASI	1	KAS	KASHI	RC	51709	39.48	75.75	1,387
	2	NAG	NAGQU	RC	55299	31.48	92.07	4,508
	3	MIN	MINQIN	RC	52681	38.63	103.08	1,367
	4	OMS	OMSK	RUS	28698	54.93	73.40	90
	5	HAI	HAILAR	RC	50527	49.25	119.70	653
	6	XIL	XILIN HOT	RC	54102	43.95	116.12	1,004
	7	QIN	QINGDAO	RC	54857	36.07	120.33	77
	8	KAG	KAGOSHIMA	J	47827	31.56	130.55	4
	9	TAT	TATENO	J	47646	36.06	140.13	25
	10	SAP	SAPPORO	J	47412	43.06	141.33	18
	11	PET	PETROPAVLOVSK	RUS	32540	53.08	158.58	78
0–30 ASI	1	KUN	KUNMING	RC	56778	25.02	102.68	1,892
	2	KOW	KOWLOON	RC	45004	22.33	114.17	24
	3	CHI	CHIANG MAI	T	48327	18.77	98.97	313
	4	ISH	ISHIGAKIJIMA	J	47918	24.34	124.16	6
0–60 AUS	1	INV	INVERCARGILL	NZ	93844	−46.41	168.32	2
	2	ADE	ADELAIDE	AUS	94672	−34.95	138.52	6
	3	PER	PERTH	AUS	94610	−31.93	115.98	20
	4	DAR	DARWIN	AUS	94120	−12.42	130.89	31
60–90 ANT	1	AMS	AMUNDSEN SCOTT	ANT	89009	−90.00	0.00	2,835
	2	CAS	CASEY	ANT	89611	−66.28	110.52	40
	3	DAV	DAVIS	ANT	89571	−68.57	77.97	18
	4	SYO	SYOWA	ANT	89532	−69.01	39.58	18

Note. Each region comprises several individual stations. The eight GRUAN stations are shown in red.

3. Radiosonde Temperature Trend Profiles

Upper-air temperature trend profiles have been calculated using data from all five data sets at all selected radiosonde stations. Several time periods have been analyzed. Figure 2 illustrates temperature trend profiles for 1976 to 2000 (left) and 2001 to 2015 (right). Trend profiles are averaged over 10 stations in Europe (30–60 EUR), 29 stations over the midlatitude NH (30–60 NH), and 4 stations over Australia/New Zealand (0–60 AUS). At most levels and regions, the temperature trend profiles for the five different data sets agree on the sign but not the magnitude of trends. In the troposphere, warming trends occur in all regions both before and after 2000. In contrast, lower stratospheric temperature trends show a pronounced change from cooling to warming at the turn of the century. This holds for all data sets used here and for each of the three regions, indicating that the reversal of the sign of the trends is robust to currently identified observational uncertainties in the radiosonde data.

Profiles of temperature trends averaged over all five data sets, for 1976 to 2000 (blue) and 2001 to 2015 (red), together with their 2σ standard errors, are presented in Figure 3. Positive trends over the period 2001 to 2015 can be observed in all regions except Antarctica (60–90 ANT). Trends are judged to be statistically significant at the 5% level if the 2σ standard error does not encompass zero trend. In the lower stratosphere, early 21st century warming trends that are significantly different from zero at the stipulated 5% level are only observed at a few regions and altitudes.

4. Ozone Recovery and Stratospheric Warming

Figure 4 shows vertical profiles of temperature and ozone trends for the four seasons and the annual mean. Results are averages for three individual European ozone measurement stations: Payerne,

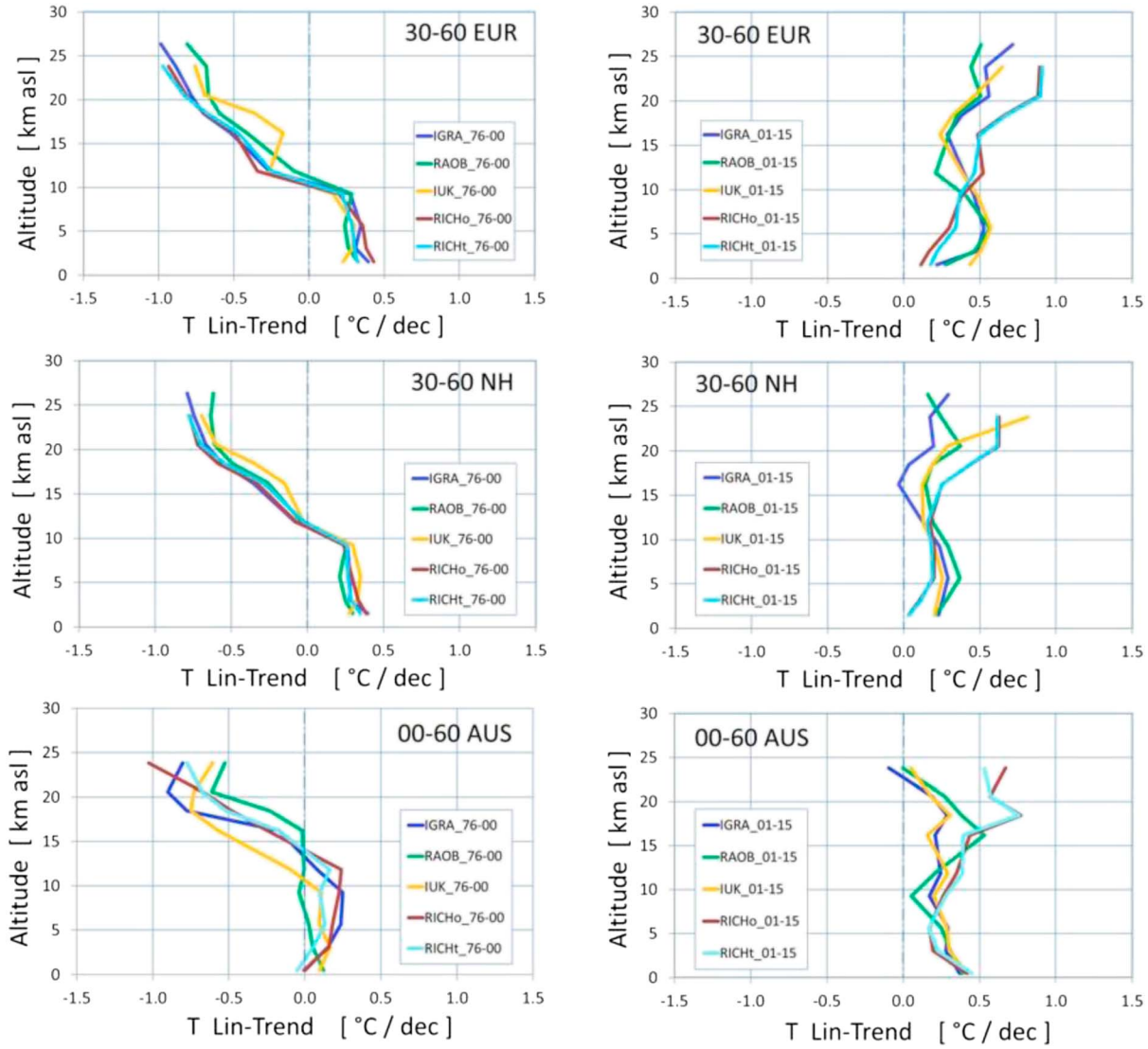

Figure 2. Temperature trend profiles for 1976–2000 (left) and 2001–2015 (right). Trend profiles are shown for the five data sets analyzed here: IGRA (dark blue), RAOBCORE (green), IUK (orange), RICH-obs (red), and RICH-tau (light blue) at 10 pressure levels from 850 to 20 hPa (~1.5- to ~26.8-km altitude; for some data sets, the highest pressure level is at 30 hPa). For presentational purposes, pressure levels have been converted to altitudes assuming a standard atmosphere. Data are shown for 30–60 EUR, 30–60 NH, and 0–60 AUS. IGRA = Integrated Global Radiosonde Archive; RAOBCORE = RAdiosonde OBservation COrrection using REanalyses; IUK = Iterative Universal Kriging; RICH = Radiosonde Innovation Composite Homogenization.

Hohenpeissenberg, and Uccle. The profiles cover 11 pressure levels from 850 to 10 hPa (~1.5- to ~30.9-km altitude) with the winter seasonal profiles averaged over December, January, February, etc. Trend profiles in the stratosphere (above 10 km), show very similar seasonal and annual changes for temperature and ozone. With the exception of the fall season, annual and seasonal profiles switch from negative to positive trends before and after the turn of the century, respectively, both for ozone and temperature. The largest trend changes occur during the winter season (blue). Changes are considerably smaller in fall (brown). Similar covarying behavior between ozone and temperature changes in the lower stratosphere has recently been observed over Antarctica (Solomon et al., 2017).

Absorption of incoming solar radiation as well as absorption of upward thermal radiation by ozone is an important determinant of stratospheric temperature. Increases in atmospheric concentrations of ODSs have depleted stratospheric ozone since the 1970s, reaching maximum ODS concentrations and ozone minima in the middle to late 1990s (depending on region). Following large reductions in ODS emissions mandated by

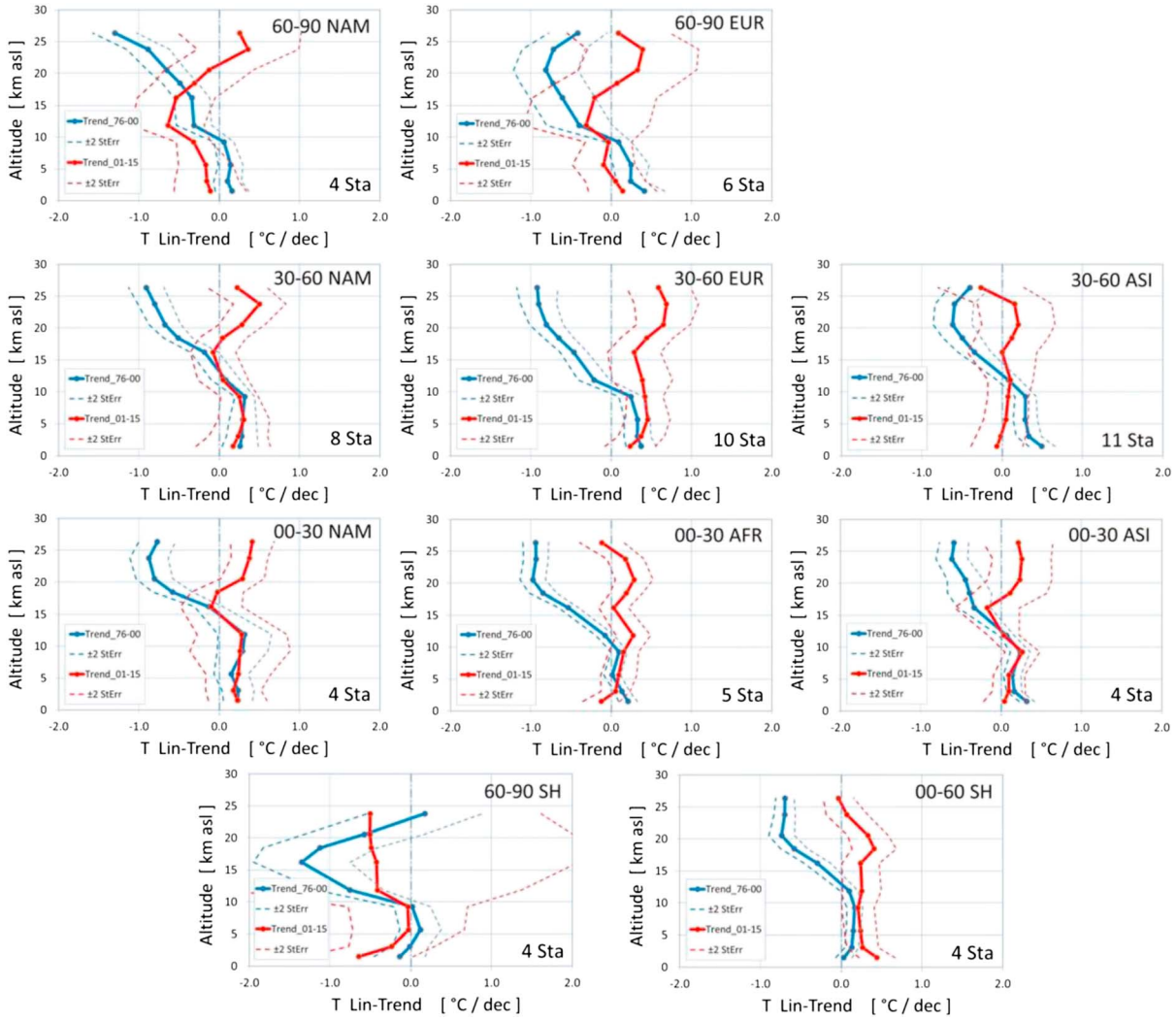

Figure 3. Temperature trend profiles averaged over all five radiosonde data sets and their respective 2σ standard errors. Results are for 1976–2000 (blue) and 2001–2015 (red). The graphs in the three upper rows show trend profiles from eight regions in the Northern Hemisphere, averaged over the number of stations indicated in the panel. In row four, profiles of two regions in the Southern Hemisphere are shown.

the Montreal Protocol, measurements at many ozone stations around the world show gradual recovery of lower stratospheric ozone (Harris, 2015; Steinbrecht et al., 2017; WMO, 2014). The observed 2001–2015 stratospheric warming is strongest around 20 to 25 km, where ozone concentrations peak and where their radiative impact on stratospheric temperatures is largest.

5. Comparison of Radiosonde and Satellite Observations

Radiosondes measure upper-air temperature profiles with high vertical resolution, whereas most satellite observations (except GPS-RO) provide estimates of the temperature of thick atmospheric layers. We use satellite data from Remote Sensing System (RSS) that merges together data from the MSU Channel 4 and AMSU Channel 9 microwave sounders to provide continuous records of lower stratospheric temperature from 1979 to 2015. We use monthly RSS V3.3 TLS values (Mears & Wentz, 2009) of the respective 2.5° × 2.5° grid point values closest to the radiosonde locations. We also use NOAA STAR Advanced Microwave Sounding Unit-A Channel 9 and Channel 10 satellite data from 1999 to 2015 (Zou & Qian, 2016). To compare satellite to radiosonde observations, radiosonde data are weighted with the satellite TLS Channel 9 weighting function, which extends from about 10 to 30 km and peaks at 16.8 km. Note that there may be missing information at the top of the radiosonde profile as the weighting function extends above the typical maximum ascent attained.

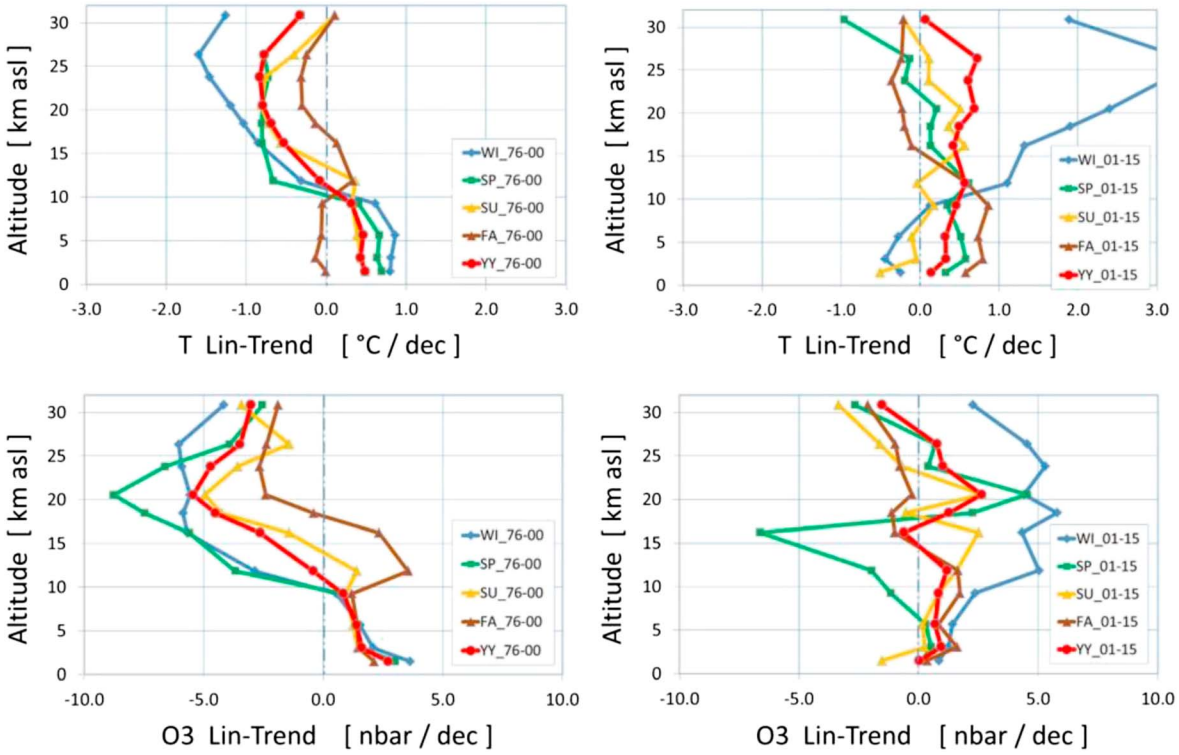

Figure 4. Annual and NH seasonal trend profiles for temperature (above) and ozone (below) for the two time periods 1976–2000 (left) and 2001–2015 (right). Trend profiles are averaged over the three European ozone stations Payerne, Hohenpeissenberg, and Uccle and are shown for pressure levels from 850 to 10 hPa (~1.5- to ~30.9-km altitude). Results are for the four seasons, winter (December, January, February; blue), spring (green), summer (orange), fall (brown), and annual (red).

NOAA STAR Channel 10 data, which peaks at 20.1 km, are also compared to radiosonde Channel 10 weighted data. The weighting functions used are from RSS and are shown in Figure 5 as they were used at the respective pressure levels of the radiosonde profiles. Averages over regions and latitude zones are made by averaging over the given radiosonde locations in the various regions and zones.

Annual mean time series of stratospheric temperature anomalies from 1979 to 2015 for radiosonde and satellite observations are shown in Figure 6. Results are for two different vertical layers (average over the 70, 50, 30 hPa pressure level and the satellite TLS level) and five spatial domains and are averages over all five radiosonde data sets. In Table 2 we show tropospheric and lower stratospheric trend values measured by radiosondes, and lower stratospheric satellite trends before and after the turn of the century. For the 1979 to 2000 period, trend values shown are averages of three linear trends calculated over the periods 1979–1999, 1979–2000, and 1979–2001. The 2000 to 2015 period is averaged over the trends computed over the 1999–2015, 2000–2015, and 2001–2015. These choices are based on the analysis of a number of different time periods. This analysis revealed that the year 2000 was a reasonable common breakpoint for the different latitudinal zones. Averaging over 1999, 2000, and 2001 reduces some of the noise associated with our specific choice of breakpoint (see also Figure 6). The values shown in Table 2 are least squares linear trends for radiosonde and satellite data, calculated using annual mean temperature anomalies. As noted above, trends are judged to be statistically significant at the 5% level if the 2σ standard error does not encompass zero trend. An overall average value over 56 stations of all regions (except Antarctica, which still shows large negative trends after 2000 for radiosonde and satellite data) is also included in Table 2.

When results from all stations (except Antarctic stations) are spatially averaged, the troposphere (the average over the 700, 500, and 300 hPa pressure levels) exhibits warming trends of +0.19 over 1979 to 2000 and +0.16 °C/decade over 2000 to 2015. Both trends are statistically significant at the 5% level. Since the turn of the century, trends have increased slightly in 0–30 NH and 0–60 AUS (Figure 3, Table 2). In the high latitudes of the Northern and Southern Hemispheres the troposphere was warming before 2000 but has been

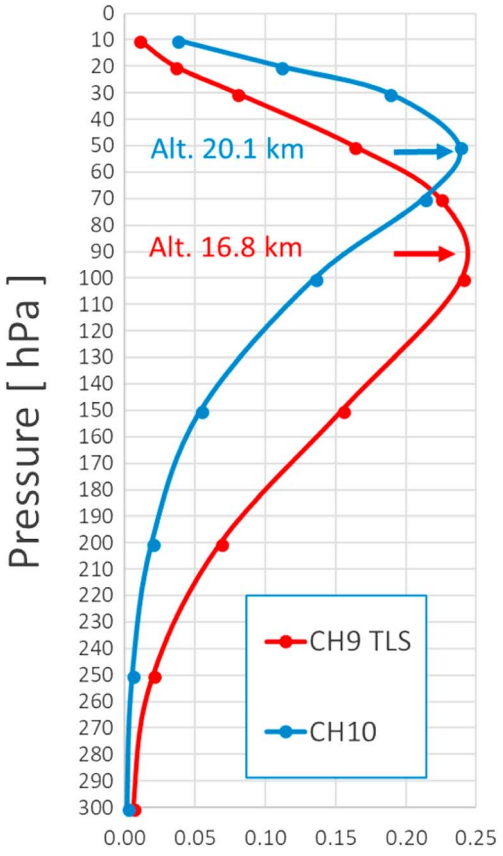

Figure 5. Channel 9 (TLS) and channel 10 satellite weighting functions that have been used for the weighting of radiosonde profiles measurements at the given pressure levels. TLS = temperature of the lower stratosphere.

cooling slightly since the turn of the century. These results are consistent with global temperature trends reported in the fifth assessment report of the Intergovernmental Panel on Climate Change (IPCC, 2013).

In the lower stratosphere, radiosonde temperature trends averaged over the 70, 50, and 30 hPa pressure levels (~18.4- to ~23.8-km altitude) change sign between the two analysis periods. The averages of all stations (excluding Antarctic stations) yield a cooling trend of −0.82 ± 0.24 °C/dec before 2000 and a warming of +0.23 ± 0.22 °C/dec over 2000 to 2015. The latter result is statistically significant at the 5% level.

TLS-weighted radiosonde and satellite trends are presented in the last three columns of Table 2. Radiosonde trends are generally reduced when applying the TLS weighting function, which peaks at 16.8-km altitude. The reduction is particularly apparent in the Northern Hemisphere where the largest trends in both periods are above 20 km (see also Figure 3). Over Australia the largest warming trends are below 20 km; in this case, weighting the radiosonde data yields a small trend increase over the 2000 to 2015 period. Overall cooling is strong between 1979 and 2000, and warming is observed in most regions after the turn of the century, but statistically significant trends at the 5% level are only found in two longitudinal zones. In most cases, satellite TLS data show smaller trends both before and after 2000. Over the 1979 to 2000 period, satellites trends are on average roughly 0.05 °C/dec smaller (less cooling) than the radiosonde trends. From 2000 to 2015, small warming trends (which do not achieve statistical significance at the 5% level) are observed in the 30–60 NH and 0–60 AUS zones for RSS satellite data, whereas NOAA data only show warming in the 30–60 NH zone. Over all regions considered here (except Antarctica), satellite TLS trends show at least 0.15 °C/dec smaller trends (i.e., show less warming) than TLS weighted radiosonde measurements.

In Table 3, NOAA AMSUA Channel 10 trends from 2000 to 2015 are compared to radiosonde Channel 10 weighted trends. In all investigated zones satellite observed trends are considerably smaller compared to those from radiosonde measurements. Averaged over all zones (except Antarctica) the difference is 0.25 °C/dec, that is, it is even larger than for the Channel 9 TLS comparisons in Table 2.

RSS satellite Channel 9 TLS trends measured at the radiosonde station locations have also been compared to RSS TLS trends averaged over the regions of interest. Table 4 shows that over most latitude zones except 60–90 NH, the station and regional-average trend values are similar; trend differences between the two types of comparison are relatively small for the period 2000 to 2015 (when results are averaged over all regions except Antarctica). This suggests that the comparison between the satellite TLS trends and the "satellite-weighted" radiosonde TLS trends is not particularly sensitive to choices made regarding subsampling satellite data at radiosonde locations.

As mentioned above, the temperature trends listed in Tables 2 and 3 result from radiosonde data averaged over all five data sets. However, trend profiles illustrated in the right panels of Figure 2 indicate that in the lower stratosphere, homogenized data show generally higher warming trends than the nonhomogenized IGRA records. Results for individual radiosonde data sets are shown in Table 5 for the period 2000 to 2015, weighted with the Channel 9 (Table 5 upper part) and Channel 10 (Table 5 central part) weighting functions. Averages for the 70-, 50-, and 30-hPa pressure levels (Table 5, lower part) are also given. Averaged over all zones (except Antarctica), the results show that in both Channels 9 and 10, and in the average over the three pressure levels, homogenized data always have larger warming trends than IGRA. RICH-obs and RICH-tau show the largest trends. The homogenized data further indicate that averaged over all zones (except Antarctica) Channel 10 weighted data show larger trends than Channel 9 weighted data sets, and largest trends are found in the nonweighted 70-, 50- and 30-hPa levels. This shows that trends observed are larger around 20 km than around 16-km altitude. Interestingly, this is contrary to the satellite records, which show

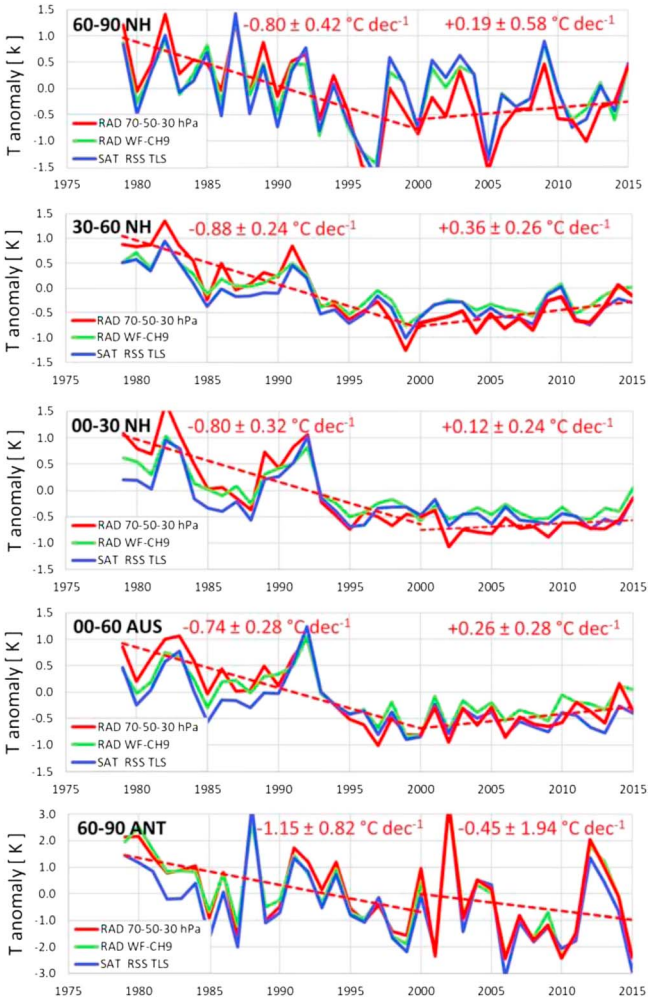

Figure 6. Annual mean temperature anomalies in the lower stratosphere for the period 1979–2015. Time series are radiosonde measurements averaged over the 70, 50, and 30 hPa pressure levels (~18.4- to ~23.8-km altitude; red), radiosonde profiles weighted with the TLS (channel 9) weighting function (green), and satellite observations at the TLS level (blue). Data are shown for 60–90 NH (10 Sta.), 30–60 NH (29 Sta.), 0–30 NH (13 Sta.), 0–60 AUS (4 Sta.), and 60–90 ANT (4 Sta.). Trend lines and trend values with their respective ±2σ standard errors are given for the radiosonde 70, 50, and 30 hPa levels for the periods 1979–2000 and 2000–2015 (red broken lines). TLS = temperature of the lower stratosphere.

lower temperature trends in Channel 10 than Channel 9. Hence, over the 2000 to 2015 period, all radiosonde data sets show higher temperature trends than satellite records, but differences are also observed between nonhomogenized and homogenized data sets.

6. Discussion

Radiosonde upper-air data show tropospheric warming in all investigated continental zones before 2000. Warming continues after 2000, except over the high latitudes of the Northern and Southern Hemispheres. In the lower stratosphere at the 70-, 50-, and 30-hPa pressure levels, radiosondes show strong cooling before 2000 and, except for Antarctica, warming trends in all latitude zones over the 2000 to 2015 period. Convolving radiosonde temperature profiles with the CH-9 TLS satellite weighting function reduces the magnitude of the trends before and after 2000. The impact of weighting the radiosonde data is largest in the Northern Hemisphere, where the strongest pre-2000 cooling trends and post-2000 warming trends are above 20-km altitude. Over both periods, TLS trends inferred from satellite observations are smaller compared to those inferred from radiosonde measurements. Homogenized radiosonde data sets show larger warming trends in the lower stratosphere than nonhomogenized data records.

Table 2
Troposphere and Lower Stratosphere Temperature Trend Values and Their Respective ±2σ Standard Errors

		Troposphere	Lower stratosphere			
Latitude zone	Sta	RAD ALL5 700-500-300 hPa	RAD ALL5 70-50-30 hPa	RAD ALL5 WF CH9 TLS	SAT RSS WF CH9 TLS	SAT NOAA WF CH9 TLS
			Trends 1979–2000 (°C/dec)			
60–90 NH	10	+0.24 ± 0.16	−0.80 ± 0.42	−0.54 ± 0.44	−0.46 ± 0.50	
30–60 NH	29	+0.24 ± 0.16	−0.88 ± 0.24	−0.55 ± 0.18	−0.59 ± 0.20	
0–30 NH	13	+0.12 ± 0.16	−0.80 ± 0.32	−0.47 ± 0.22	−0.34 ± 0.30	
0–60 AUS	4	+0.10 ± 0.18	−0.74 ± 0.28	−0.45 ± 0.26	−0.39 ± 0.32	
60–90 ANT	4	+0.15 ± 0.26	−1.15 ± 0.82	−1.32 ± 0.70	−0.85 ± 0.84	
AVERAGE exc. ANT	56	+0.19 ± 0.12	−0.82 ± 0.24	−0.51 ± 0.20	−0.46 ± 0.24	
			Trends 2000–2015 (°C/dec)			
60–90 NH	10	−0.06 ± 0.26	+0.19 ± 0.58	−0.04 ± 0.60	−0.13 ± 0.66	−0.12 ± 0.66
30–60 NH	29	+0.24 ± 0.20	+0.36 ± 0.26	+0.24 ± 0.20	+0.08 ± 0.26	+0.10 ± 0.26
0–30 NH	13	+0.21 ± 0.20	+0.12 ± 0.24	+0.09 ± 0.18	−0.05 ± 0.20	−0.04 ± 0.20
0–60 AUS	4	+0.19 ± 0.22	+0.26 ± 0.28	+0.31 ± 0.24	+0.05 ± 0.24	−0.08 ± 0.26
60–90 ANT	4	−0.05 ± 0.46	−0.45 ± 1.94	−0.37 ± 1.88	−0.65 ± 1.92	−0.78 ± 1.60
AVERAGE exc. ANT	56	+0.16 ± 0.16	+0.23 ± 0.22	+0.14 ± 0.20	−0.01 ± 0.24	−0.04 ± 0.24

Note. Results are averages of station values in the five latitudinal zones and are also averaged over all zones except Antarctica. Trends were calculated over the time periods 1979–2000 and 2000–2015. Lower stratosphere trends are given for the 70, 50, and 30 hPa pressure level measured by the radiosondes and for Channel 9 TLS weighted radiosonde and RSS and NOAA satellite observations. Statistically significant trends are shown in red.

That observations at the satellite Channels 9 and 10 levels show only minor or no warming trends at the radiosonde station locations, and similar or even slightly lower trends over the entire investigated regions is consistent with results of recent analyses of near-global satellite observations (McLandress et al., 2015; Randel et al., 2016; Seidel et al., 2016) over the data record 1979 to 2015. The satellite SSU channels measuring global average temperature anomalies in the middle and upper stratosphere show strong cooling before 1998 and minor cooling thereafter (McLandress et al., 2015). The MSU Channel 4 temperature retrieval, which represents a weighted mean of the temperatures in the lower stratosphere between 15 and 30 km, shows cooling before 1998, but no significant trend thereafter (Randel et al., 2016; Seidel et al., 2016). The lower stratosphere temperature retrievals for AMSU Channels 9 and 10 also show no clear trends since the turn of the century (McLandress et al., 2015; Seidel et al., 2016). The lower trends in satellite observations after the turn of the century could partly be due to the large vertical extent of the weighting functions, which sample part of the middle stratosphere that is still cooling. This could also explain why AMSU Channel 10 shows more negative trends than AMSU Channel 9. A positive bias of temperature trends above 100 hPa has recently also been observed between radiosonde and GPS-RO data (Ho et al., 2017), whereas AMSU Channel 10 and GPS-RO data agree well and show no trends from 2002 to 2016 (Khaykin et al., 2017).

Table 3
Radiosonde Channel 10 Weighted and NOAA AMSUA Channel 10 Data for the Period 2000–2015

		Trends 2000–2015 (°C/dec)	
Latitude zone	Sta	RAD ALL5 WF CH10	SAT NOAA WF CH10
60–90 NH	10	+0.10 ± 0.50	+0.00 ± 0.58
30–60 NH	29	+0.30 ± 0.22	+0.07 ± 0.28
0–30 NH	13	+0.09 ± 0.16	−0.10 ± 0.22
0–60 AUS	4	+0.19 ± 0.24	−0.24 ± 0.24
60–90 ANT	4	−0.37 ± 1.70	−0.93 ± 1.84
AVERAGE exc. ANT	56	+0.18 ± 0.18	−0.07 ± 0.22

Depending on scenarios of the future evolution of lower stratospheric ozone concentrations, models project further stratospheric cooling (Shepherd & Jonsson, 2008; Thompson & Solomon, 2009) or no significant stratospheric temperature trends over coming decades (Ferraro et al., 2015; Stolarski et al., 2010). A recent study isolating the roles of different forcing agents in global stratospheric temperature change was made using model simulations with incrementally added single forcings (Aquila et al., 2016). This study found that the cooling of the middle and upper stratosphere from 1979 to the present is mostly driven by changes in GHG concentrations (predominantly CO_2). In the lower stratosphere, cooling from 1979 to the end of the twentieth century is primarily driven by increases in ODS concentrations. They concluded that over the full satellite era, the middle and upper stratosphere is still expected to

Table 4
Lower Stratosphere Temperature Trends From the RSS Satellite Channel 9 TLS Observations at the Radiosonde Station Locations Compared to Observations Over the Entire Regions for the Period 2000–2015

		2000–2015	
		SAT RSS WF CH9 TLS	SAT RSS WF CH9 TLS
Latitude zone	Sta	at stations	over region
60–90 NH	10	−0.13 ± 0.66	−0.24 ± 0.64
30–60 NH	29	+0.08 ± 0.26	+0.04 ± 0.24
0–30 NH	13	−0.05 ± 0.20	−0.01 ± 0.24
0–60 AUS	4	+0.05 ± 0.24	+0.05 ± 0.20
60–90 ANT	4	−0.65 ± 1.92	−0.58 ± 1.60
AVERAGE exc. ANT	56	−0.01 ± 0.24	−0.04 ± 0.22

cool and that after 2000 the lower stratosphere should show only minor cooling or even warming trends in response to the combined effects of GHG and ODS forcing.

Numerous studies have shown that stratospheric temperature is driven by radiative heating processes involving O_3, CO_2, and water vapor (Gettelmann et al., 2004), by the Brewer-Dobson circulation (Butchart, 2014) and by external forcing such as the solar cycle or volcanic eruptions (Fujiwara et al., 2015; Mitchell et al., 2015; Vernier et al., 2011). The observed positive temperature trends in the lower stratosphere may be explained using a simple one-dimensional radiative transfer model where energy transfer is determined primarily by three processes (Andrews et al., 1987; Gettelmann et al., 2004; London, 1980).

1. Shortwave heating by O_3 (absorption of downward solar radiation)
2. Longwave cooling by CO_2 (emission of outgoing thermal radiation)
3. Longwave heating by O_3 (absorption of upward thermal radiation from the troposphere)

At around 15-km altitude, cooling and heating rates from all three radiative processes are weak. At higher altitudes, shortwave heating by O_3 and longwave cooling by CO_2 increase but balance such that their net effect remains close to zero. However, longwave heating by O_3 warms the lower stratosphere and this heating peaks between 20- and 25-km altitude. Above 30 km, longwave heating by O_3 turns to longwave cooling. With rising GHG concentrations and decreasing stratospheric ozone from the 1970s to the end of the century, all three processes cooled the lower stratosphere. However, with decreasing ODSs and related ozone recovery shortwave heating by O_3 now contributes to warming. In addition, longwave heating by O_3 contributes to warming predominantly around 20- to 25-km altitude.

Table 5
Temperature Trends Calculated for 2000–2015 for All Five Radiosonde Data Sets for Channels 9 and 10 Weighted, and for the 70-, 50-, and 30-hPa Pressure Level Averaged

		Trends 2000–2015 (°C/dec)				
		IGRA	RAOBCORE	IUK	RICH-obs	RICH-tau
Latitude zone	Sta	WF CH9	WF CH9	WF CH9	WF CH9	WF CH9
60–90 NH	10	−0.08 ± 0.58	−0.04 ± 0.60	+0.03 ± 0.66	−0.02 ± 0.58	−0.08 ± 0.64
30–60 NH	29	+0.09 ± 0.20	+0.25 ± 0.22	+0.21 ± 0.20	+0.33 ± 0.20	+0.32 ± 0.20
0–30 NH	13	−0.11 ± 0.16	−0.03 ± 0.18	+0.14 ± 0.18	+0.24 ± 0.18	+0.22 ± 0.18
0–60 AUS	4	+0.22 ± 0.22	+0.23 ± 0.28	+0.22 ± 0.24	+0.43 ± 0.28	+0.44 ± 0.28
60–90 ANT	4	−0.48 ± 2.08	−0.49 ± 1.96	−0.73 ± 1.58	−0.05 ± 1.92	−0.11 ± 1.84
AVERAGE exc. ANT	56	+0.02 ± 0.20	+0.09 ± 0.20	+0.15 ± 0.22	+0.23 ± 0.20	+0.21 ± 0.22
		IGRA WF CH10	RAOBCORE WF CH10	IUK WF CH10	RICH-obs WF CH10	RICH-tau WF CH10
60–90 NH	10	+0.09 ± 0.48	+0.10 ± 0.58	+0.15 ± 0.56	+0.12 ± 0.48	+0.06 ± 0.54
30–60 NH	29	+0.16 ± 0.24	+0.35 ± 0.26	+0.27 ± 0.20	+0.37 ± 0.22	+0.37 ± 0.20
0–30 NH	13	−0.09 ± 0.18	−0.06 ± 0.20	+0.10 ± 0.20	+0.28 ± 0.18	+0.24 ± 0.16
0–60 AUS	4	+0.16 ± 0.20	+0.15 ± 0.24	+0.17 ± 0.22	+0.34 ± 0.26	+0.37 ± 0.26
60–90 ANT	4	−0.48 ± 1.90	−0.16 ± 2.82	−0.71 ± 1.42	−0.07 ± 1.76	−0.12 ± 1.66
AVERAGE exc. ANT	56	+0.06 ± 0.18	+0.11 ± 0.20	+0.18 ± 0.18	+0.28 ± 0.18	+0.26 ± 0.18
		IGRA 70–50-30 hP	RAOBCORE 70–50-30 hP	IUK 70–50-30 hP	RICH-obs 70–50-30 hP	RICH-tau 70–50-30 hPa
60–90 NH	10	+0.08 ± 0.50	+0.16 ± 0.64	+0.29 ± 0.68	+0.27 ± 0.56	+0.18 ± 0.62
30–60 NH	29	+0.13 ± 0.26	+0.27 ± 0.28	+0.40 ± 0.28	+0.51 ± 0.28	+0.51 ± 0.28
0–30 NH	13	−0.14 ± 0.24	−0.08 ± 0.24	+0.10 ± 0.28	+0.40 ± 0.24	+0.33 ± 0.22
0–60 AUS	4	+0.13 ± 0.24	+0.22 ± 0.26	+0.18 ± 0.30	+0.36 ± 0.32	+0.43 ± 0.34
60–90 ANT	4	−0.56 ± 2.06	−0.50 ± 2.16	−0.87 ± 1.66	−0.11 ± 2.10	−0.17 ± 1.98
AVERAGE exc. ANT	56	+0.03 ± 0.20	+0.12 ± 0.22	+0.25 ± 0.24	+0.40 ± 0.22	+0.37 ± 0.24

7. Conclusions

The reversal from ozone depletion to ozone recovery is likely an important driver for the lower stratospheric temperature trends to switch from cooling to warming, as also emphasized by Maycock (2016) and Solomon et al. (2017). Vertical trend profiles derived from radiosonde temperature data show maximum cooling before 2000 and maximum warming trends after 2000, predominantly at altitudes between 20 and 25 km (Figure 3). Here the longwave cooling and heating, respectively, by ozone is large, supporting the importance of ozone during the cooling and warming period before and after the turn of the century evident in radiosonde records. Furthermore, the seasonal coherence of trend changes in both ozone and temperature trends observed over Europe (Figure 4) and Antarctica (Solomon et al., 2017) suggest a link between the observed ozone and temperature trend reversal. Recently reported evidence from satellite measurements that ozone in the lower stratosphere between 60°S and 60 N has continued to decline since 1998 (Ball et al., 2018) is not supported by our results.

Although radiosonde and satellite observations show similar warming trends in the troposphere between 1979 and 2015, the radiosonde-observed switch to warming in the lower stratosphere after the turn of the century contrasts with satellite observations, which exhibit no significant trends in recent years. In most cases, TLS trend results published for satellite near-global-averages are similar to satellite trends averaged over regions of interest and also right above the radiosonde station locations (Table 4). Temperature trends from 2000 to 2015 calculated with RSS and NOAA STAR TLS Channel 9 data are 0.15 °C/dec and 0.18 °C/dec (respectively) lower than Channel 9 weighted radiosonde trends averaged over all radiosonde data sets and all stations except Antarctica (Table 2). Comparisons between NOAA STAR Channel 10 and radiosonde Channel 10 weighted trends show differences of 0.25 °C/dec (average except Antarctica) with the radiosonde-derived trends showing positive warming in all latitude zones except Antarctica (Table 3).

Our main results are as follows: (i) radiosondes show that the temperature of the lower stratosphere was cooling before around 2000 and warmed after around 2000. (ii) TLS trends from satellite observations are weaker than from radiosonde measurements, both for the cooling and the warming period. (iii) Homogenized radiosonde data show even higher TLS warming trends since 2000 than those based on nonhomogenized radiosonde records and are statistically significant over several latitudinal zones (Table 5). The difference between satellite and radiosonde-observed trends may, in part, be related to compensating continued cooling from above the radiosonde altitude range. Further investigations will be needed to resolve the discrepancy between radiosonde and the satellite temperature trends. Such work will help to improve scientific understanding of the evolution of lower stratospheric temperature.

Acknowledgments

We would like to acknowledge the authors and the staff of the different data archives, from which data were downloaded for this analysis: The Integrated Global Radiosonde Archive (IGRA) from the NOAA National Centers for Environmental Information (https://www.ncdc.noaa.gov/data-access/weather-balloon/integrated-global-radiosonde-archive); the RAdiosonde OBservation COrrection using REanalyses (RAOBCORE) archive from the University of Vienna (http://www.univie.ac.at/theoret-met/research/raobcore/); the Iterative Universal Kriging (IUK) archive at the University of New South Wales, Sydney (http://web.science.unsw.edu.au/~stevensherwood/radproj/index.html); and the Radiosonde Innovation Composite Homogenization (RICH) archive from the University of Vienna for their RICH-obs and RICH-tau data sets (http://www.univie.ac.at/theoret-met/research/raobcore/). We are also very thankful for the satellite data sets from: Remote Sensing System (RSS; http://www.remss.com/measurements/) and NOAA STAR Center for Satellite Applications and Research (https://www.star.nesdis.noaa.gov/smcd/emb/mscat/). This paper has been reviewed by several journals. The authors would like to thank the different reviewers for their positive inputs, which greatly helped to improve the manuscript. We are particularly indebted to Ben Santer for his constructive and very helpful signed review. The authors are also thankful to the Editor of JGR William Randel for supporting our work.

References

Andrews, D. G., Holton, J. R., & Leovy, C. B. (1987). *Middle atmospheric dynamics* (p. 489). San Diego, CA: Academic Press.

Aquila, V., Swartz, W. H., Waugh, D. W., Colarco, P. R., Pawson, S., Polvani, L. M., & Stolarski, R. S. (2016). Isolating the roles of different forcing agents in global stratospheric temperature changes using model integrations with incrementally added single forcings. *Journal of Geophysical Research: Atmospheres*, *121*, 8067–8082. https://doi.org/10.1002/2015JD023841

Ball, W. T., Alsing, J., Mortlock, D. J., Staehelin, J., Haigh, J. D., Peter, T., et al. (2018). Evidence for a continuous decline in lower stratospheric ozone offsetting ozone layer recovery. *Atmospheric Chemistry and Physics*, *18*(2), 1379–1394. https://doi.org/10.5194/acp-18-1379-2018

Bandoro, J., Solomon, S., Santer, B. D., Kinnison, D., & Mills, M. (2018). Detectability of the impacts of ozone-depleting substances and greenhouse gases upon global stratospheric ozone accounting for nonlinearities in historical forcings. *Atmospheric Chemistry and Physics*, *18*(1), 143–166. https://doi.org/10.5194/acp-18-143-2018

Bodeker, G. E., Bojinski, S., Cimini, D., Dirksen, R. J., Haeffelin, M., Hannigan, J. W., et al. (2016). Reference upper-air observations for climate: From concept to reality. *Bulletin of the American Meteorological Society*, *97*(1), 123–135. https://doi.org/10.1175/BAMS-D-14-00072.1

Butchart, N. (2014). The Brewer-Dobson circulation. *Reviews of Geophysics*, *52*, 157–184. https://doi.org/10.1002/2013RG000448

Dee, D. P., Uppala, S. M., Simmons, A. J., Berrisford, P., Poli, P., Kobayashi, S., et al. (2011). The ERA-interim reanalysis: Configuration and performance of the data assimilation system. *Quarterly Journal of the Royal Meteorological Society*, *137*(656), 553–597. https://doi.org/10.1002/qj.828

Durre, I., Vose, R. S., & Wuertz, D. B. (2006). Overview of the integrated global radiosonde archive. *Journal of Climate*, *19*(1), 53–68. https://doi.org/10.1175/JCLI3594.1

Ferraro, A. J., Collins, M., & Lambert, F. H. (2015). A hiatus in the stratosphere? *Nature Climate Change*, *5*(6), 497–498. https://doi.org/10.1038/nclimate2624

Fujiwara, M., Hibino, T., Mehta, S. K., Gray, L., Mitchell, D., & Anstey, J. (2015). Global temperature response to the major volcanic eruptions in multiple reanalysis data sets. *Atmospheric Chemistry and Physics*, *15*(23), 13,507–13,518. https://doi.org/10.5194/acp-15-13507-2015

Gettelmann, A., Forster, P. M. D. F., Fujiwara, M., Fu, Q., VöMel, H., Gohar, L. K., et al. (2004). Radiation balance of the tropical tropopause layer. *Journal of Geophysical Research*, *109*, D07103. https://doi.org/10.1029/2003JD004190

Gillett, N. P., Akiyoshi, H., Bekki, S., Braesicke, P., Eyring, V., Garcia, R., et al. (2011). Attribution of observed changes in stratospheric ozone and temperature. *Atmospheric Chemistry and Physics*, *11*(2), 599–609. https://doi.org/10.5194/acp-11-599-2011

GUAN (2014). http://www.wmo.int/pages/prog/gcos/documents/GUAN_Stations_Region_2014.pdf
Haimberger, L. (2007). Homogenization of radiosonde temperature time series using innovation statistics. *Journal of Climate*, *20*(7), 1377–1403. https://doi.org/10.1175/JCLI4050.1
Haimberger, L., Tavolato, C., & Sperka, S. (2012). Homogenization of the global radiosonde temperature dataset through combined comparison with reanalysis background series and neighboring stations. *Journal of Climate*, *25*(23), 8108–8131. https://doi.org/10.1175/JCLI-D-11-00668.1
Harris, N. R. P. (2015). Past changes in the vertical distribution of ozone—Part 3: Analysis and interpretation of trends. *Atmospheric Chemistry and Physics*, *15*(17), 9965–9982. https://doi.org/10.5194/acp-15-9965-2015
Ho, S.-P., Peng, L., & Vömel, H. (2017). Characterization of the long-term radiosonde 409 temperature biases in the upper troposphere and lower stratosphere using COSMIC 410 and Metop-A/GRAS data from 2006 to 2014. *Atmospheric Chemistry and Physics*, *17*, 4493–4511.
Intergovernmental Panel on Climate Change (IPCC) (2013). In T. F. Stocker, et al. (Eds.), *Climate Change 2013: The physical science basis. Contribution of Working Group I to the Fifth Assessment Report of the Intergovernmental Panel on Climate Change* (p. 1535). Cambridge, United Kingdom and New York, NY: Cambridge University Press.
Khaykin, S. M., Funatsu, B. M., Hauchecorne, A., Godin-Beekmann, S., Claud, C., Keckhut, P., et al. (2017). Postmillennium changes in stratospheric temperature consistently resolved by GPS radio occultation and AMSU observations. *Geophysical Research Letters*, *44*, 7510–7518. https://doi.org/10.1002/2017GL074353
Langematz, U., Kunze, M., Kruger, K., Labitzke, K., & Roff, G. L. (2003). Thermal and dynamical changes of the stratosphere since 1979 and their link to ozone and CO_2 changes. *Journal of Geophysical Research*, *108*(D1), 4027. https://doi.org/10.1029/2002JD002069
London, J. (1980). Radiative energy sources and sinks in the stratosphere and mesosphere. In M. Nicolet & A. C. Aikin (Eds.), *Atmospheric ozone and its variation and human influences*, Proceedings of the NATO Advanced Study Institute held 1–13 October, 1979 in Aldeia das Acoteias, Portugal (p. 703). Washington, DC: US Department of Transportation.
Maycock, A. C. (2016). The contribution of ozone to future stratospheric temperature trends. *Geophysical Research Letters*, *43*, 4609–4616. https://doi.org/10.1002/2016GL068511
McLandress, C., Shepherd, T. G., Jonsson, A. I., Clarmann, v. T., & Funke, B. (2015). A method for merging nadir-sounding climate records, with an application to the global-mean stratospheric temperature data sets from SSU and AMSU. *Atmospheric Chemistry and Physics*, *15*(16), 9271–9284. https://doi.org/10.5194/acp-15-9271-2015
Mears, C. A., & Wentz, F. J. (2009). Construction of the remote sensing systems V3.2 atmospheric temperature records from the MSU and AMSU microwave sounders. *Journal of Atmospheric and Oceanic Technology*, *26*(6), 1040–1056. https://doi.org/10.1175/2008JTECHA1176.1
Mitchell, D. M., Gray, L. J., Fujiwara, M., Hibino, T., Anstey, J. A., Ebisuzaki, W., et al. (2015). Signatures of naturally induced variability in the atmosphere using multiple reanalysis datasets. *Quarterly Journal of the Royal Meteorological Society*, *141*(691), 2011–2031. https://doi.org/10.1002/qj.2492
Polvani, L. M., Wang, L., Aquila, V., & Waugh, D. W. (2017). The impact of ozone-depleting substances on tropical upwelling, as revealed by the absence of lower-stratospheric cooling since the late 1990s. *Journal of Climate*, *30*(7), 2523–2534. https://doi.org/10.1175/JCLI-D-16-0532.1
Ramaswamy, V., Chanin, M. L., Angell, J., Barnett, J., Gaffen, D., Gelman, M., et al. (2001). Stratospheric temperature trends: Observations and model simulations. *Reviews of Geophysics*, *39*(1), 71–122. https://doi.org/10.1029/1999RG000065
Ramaswamy, V., Schwarzkopf, M. D., Randel, W. J., Santer, B. D., Soden, B. J., & Stenchikov, G. L. (2006). Anthropogenic and natural influences in the evolution of lower stratospheric cooling. *Science*, *311*(5764), 1138–1141. https://doi.org/10.1126/science.1122587
Randel, W. J., Shine, K. P., Austin, J., Barnett, J., Claud, C., Gillett, N. P., et al. (2009). An update of observed stratospheric temperature trends. *Journal of Geophysical Research*, *114*, D02107. https://doi.org/10.1029/2008JD010421
Randel, W. J., Smith, A. K., Wu, F., Zou, C. Z., & Qian, H. (2016). Stratospheric temperature trends over 1979–2015 derived from combined SSU, MLS, and SABER satellite observations. *Journal of Climate*, *29*(13), 4843–4859. https://doi.org/10.1175/JCLI-D-15-0629.1
Santer, B. D., Painter, J. F., Mears, C. A., Doutriaux, C., Caldwell, P., Arblaster, J. M., et al. (2013). Identifying human influences on atmospheric temperature. *PNAS*, *110*(1), 26–33. https://doi.org/10.1073/pnas.1210514109
Santer, B. D., Wehner, M. F., Wigley, T. M., Sausen, R., Meehl, G. A., Taylor, K. E., et al. (2003). Contributions of anthropogenic and natural forcing to recent tropopause height changes. *Science*, *301*(5632), 479–483. https://doi.org/10.1126/science.1084123
Seidel, D. J., Mears, C., Moradi, I., & Zou, C.-Z. (2016). Stratospheric temperature changes during the satellite era. *Journal of Geophysical Research: Atmospheres*, *121*, 664–681. https://doi.org/10.1002/2015JD024039
Seidel, D. J., Gillett, N. P., Lanzante, J. R., Shine, K. P., & Thorne, P. W. (2011). Stratospheric temperature trends: Our evolving understanding. *Reviews Climate Change*, *2*, 592–616.
Shepherd, T. G., & Jonsson, A. I. (2008). On the attribution of stratospheric ozone and temperature changes to changes in ozone-depleting substances and well-mixed greenhouse gases. *Atmospheric Chemistry and Physics*, *8*(5), 1435–1444. https://doi.org/10.5194/acp-8-1435-2008
Sherwood, S. C., & Nishant, N. (2015). Atmospheric changes through 2012 as shown by iteratively homogenized radiosonde temperature and wind data (IUKv2). *Environmental Research Letters*, *10*(5), 054007. https://doi.org/10.1088/1748-9326/10/5/054007
Shine, K. P., Barnett, J. J., & Randel, W. J. (2008). Temperature trends derived from stratospheric sounding unit radiances: The effect of increasing CO_2 on the weighting function. *Geophysical Research Letters*, *35*, L02710. https://doi.org/10.1029/2007GL032218
Shine, K. P., Bourqui, M. S., Forster, P. M. F., Hare, S. H. E., Langematz, U., Braesicke, P., et al. (2003). A comparison of model-simulated trends in stratospheric temperatures. *Quarterly Journal of the Royal Meteorological Society*, *129*(590), 1565–1588. https://doi.org/10.1256/qj.02.186
Solomon, S., Ivy, D., Gupta, M., Bandoro, J., Santer, B., Fu, Q., et al. (2017). Mirrored changes in Antarctic ozone and stratospheric temperature in the late 20th versus early 21st centuries. *Journal of Geophysical Research: Atmospheres*, *122*, 8940–8950. https://doi.org/10.1002/2017JD026719
Solomon, S. K., Rosenlof, K. H., Portmann, R. W., Daniel, J. S., Davis, S. M., Sanford, T. J., & Plattner, G.-K. (2010). Contributions of stratospheric water vapor to decadal changes in the rate of global warming. *Science*, *327*(5970), 1219–1223. https://doi.org/10.1126/science.1182488
Steinbrecht, W., Froidevaux, L., Fuller, R., Wang, R., Anderson, J., Roth, C., et al. (2017). An update on ozone profile trends for the period 2000 to 2016. *Atmospheric Chemistry and Physics*, *17*(17), 10,675–10,690. https://doi.org/10.5194/acp-17-10675-2017
Stolarski, R. S., Douglass, A. R., Newman, P. A., Pawson, S., & Schoeberl, M. R. (2010). Relative contribution of greenhouse gases and ozone-depleting substances to temperature trends in the stratosphere: A chemistry–climate model study. *Journal of Climate*, *23*(1), 28–42. https://doi.org/10.1175/2009JCLI2955.1
Thompson, D. W. J., Seidel, D. J., Randel, W. J., Zou, C. Z., Butler, A. H., Mears, C., et al. (2012). The mystery of recent stratospheric temperature trends. *Nature*, *491*(7426), 692–697. https://doi.org/10.1038/nature11579
Thompson, D. W. J., & Solomon, S. (2009). Understanding recent stratospheric climate change. *Journal of Climate*, *22*(8), 1934–1943. https://doi.org/10.1175/2008JCLI2482.1

Vernier, J. P., Thomason, L. W., Pommereau, J.-P., Bourassa, A., Pelon, J., Garnier, A., et al. (2011). Major influence of tropical volcanic eruptions on the stratospheric aerosol layer during the last decade. *Geophysical Research Letters*, *38*, L12807. https://doi.org/10.1029/2011GL047563

World Meteorological Organization (WMO) (2014). Scientific assessment of ozone depletion: 2014, WMO, global ozone research and monitoring project, Report No. 55, 416 pp., Geneva, Switzerland.

Zhao, L., Xu, J., Powell, A. M., Jiang, Z., & Wang, D. (2016). Use of SSU/MSU satellite observations to validate upper atmospheric temperature trends in CMIP5 simulations. *Remote Sensing*, *8*, 13.

Zou, C.-Z., & Qian, H. (2016). Stratospheric temperature climate data record from merged SSU and AMSU-A observations. *Journal of Atmospheric and Oceanic Technology*, *33*(9), 1967–1984. https://doi.org/10.1175/JTECH-D-16-0018.1